Nonlinear Conductivity of Geometrically Frustrated Iridate $Ca_5Ir_3O_{12}$

Kazuyuki Matsuhira[1]*, Kazuma Nakamura[1], Yuki Yasukuni[1], Yoshihide Yoshimoto[2], Daigorou Hirai[3], Zenji Hiroi[3]

[1] *Graduate School of Engineering, Kyushu Institute of Technology, Kitakyushu 804-8550, Japan*

[2] *Graduate School of Information Science and Technology, University of Tokyo, Tokyo 113-0033, Japan*

[3] *Institute for Solid State Physics, University of Tokyo, Kashiwa 277-8581, Japan*

(Received December 20, 2017)

We report the discovery of nonlinear conductivity along the c-axis in a single crystal of $Ca_5Ir_3O_{12}$, which indicates a semiconducting behavior with a narrow band gap of ∼0.2 eV. The resistivity decreases with increase in the applied current. This nonlinearity is reversible with the direction of current. We also show the *ab initio* density functional band structures and the Fermi surface. We found that the spin-orbit interactions result in an appreciable change in the low-energy electronic structure; the interaction splits the metallic bands and leads to a pocket-like band structure, thus reducing the metallic trend. The size of the spin-orbit interaction is estimated as ∼0.3 eV, which is large enough to be comparable to the valence bandwidth of ∼0.5 eV. The Fermi surface exhibits a sheet structure along the c^*-axis, due to the 1D chain structure of edge-sharing IrO_6.

Studies on the physical properties of Ir oxides for the last ten years have revealed the importance of spin-orbit interaction (SOI).[1,2)] In particular, in the case of Ir^{4+} ($5d^5$), the strong SOI splits the sixfold degenerate t_{2g} states into the occupied $J_{eff} = 3/2$ and half-occupied $J_{eff} = 1/2$ states.[1,3)] The bands formed by the $J_{eff} = 1/2$ states are narrower than the width of the whole t_{2g} band in the absence of SOI, and consequently the system can easily become a Mott-insulating state with even a moderate amount of correlations on the 5d electrons; the Mott-insulating state in Sr_2IrO_4 has been well studied as a typical case.[1,3)] Recently, there has been a considerable increase in the research on

*E-mail address: matuhira@elcs.kyutech.ac.jp

Ir oxides because of their attractive physical properties, such as Kitaev spin liquid in A_2IrO_3, spontaneous Hall effect at zero field in $Pr_2Ir_2O_7$, metal-insulator transitions with all-in all-out ordering in $Ln_2Ir_2O_7$, and the prediction of superconducting state due to carrier doping for the SOI induced Mott-insulating state in Sr_2IrO_4.[4–11)]

$Ca_5Ir_3O_{12}$ has a hexagonal structure with space group of $P\bar{6}2m$ (No. 189), which is shown in Fig.1(a).[12,13)] In the crystal structure, it should be noted that one-dimensional (1D) chains of the edge-sharing IrO_6 form triangular lattices (Figs.1(b) and (c)). The averaged valence of Ir ions in $Ca_5Ir_3O_{12}$ is +4.67. It is reported that $Ca_5Ir_3O_{12}$ exhibits semiconductivity and an antiferromagnetic ordering below 7.8 K.[12,15,17)] In addition, $Ca_5Ir_3O_{12}$ exhibits a second order phase transition at 105 K, where the specific heat shows a sharp anomaly and the electrical resistivity shows a sharp bending. The origin of the phase transition at 105 K is not clear at present, as the structural and magnetic transitions have not been confirmed in XRD, neutron scattering and μSR experiments for the powder samples;[12,17)] therefore, we will not refer to the origin of phase transition in this paper.

In this letter, firstly, we report the transport properties along the c-axis in a single crystal of $Ca_5Ir_3O_{12}$. We have discovered nonlinear conductivity in its current-voltage relationship. In order to study the transport property, it is necessary to clarify how important SOI is in the band structure of $Ca_5Ir_3O_{12}$. We also show the *ab initio* density functional band structures and Fermi surface, and discuss the features of the observed nonlinear conductivity and the calculated band structure.

Single crystals of $Ca_5Ir_3O_{12}$ were grown by the $CaCl_2$ flux method. They were grown in a Pt crucible from the mixture of polycrystalline $Ca_5Ir_3O_{12}$ with $CaCl_2$ flux in a ratio of 1:30; the polycrystalline sample of $Ca_5Ir_3O_{12}$ weas synthesized by a standard solid-state reaction, as reported previously.[12)] The mixtures were heated to 1423 K and annealed for 12 h. The temperature was decreased to 1003 K at a rate of 1 K/h. Fig1.(d) shows the typical needle like crystals. We confirmed that the grown crystals are identified to $Ca_5Ir_3O_{12}$ by powder X-ray diffraction measurement for powder sample obtained from a few crystals. The estimated lattice parameters a and c were 9.4191 Å and 3.1963 Å, respectively. These values are in agreement with the values reported previously.[12,15)]

The electrical resistivity and current-voltage (I-V) characteristic of a single crystal was measured by a four-probe method using GM refrigerator. The sample was fixed to the copper plate, which was insulated using a Kapton tape with GE varnish. The

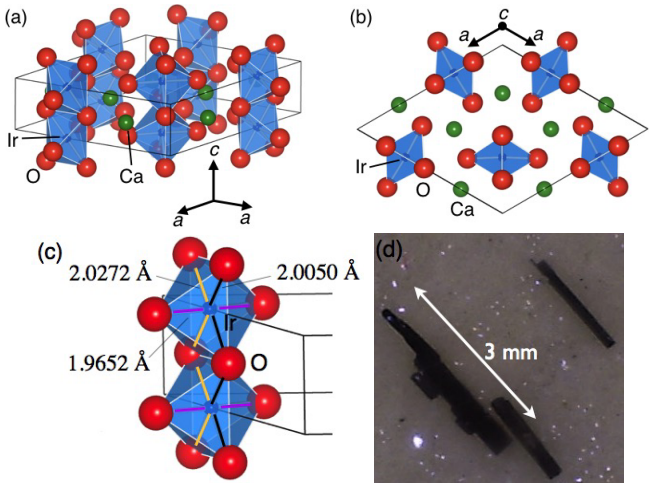

Fig. 1. (Color online) (a) Crystal structure of $Ca_5Ir_3O_{12}$. (b) Sublattice of Ir form triangular lattices in the c-plane. (c) 1D chains of the edge-sharing IrO_6 along the c-axis. The bond length between O and Ir obtained from the structure parameters in ref.12 are shown. These structural images were produced by VESTA.[14] (d) Single crystal of $Ca_5Ir_3O_{12}$ grown by a flux method. The long direction of the crystal corresponds to the c-axis.

terminal was fixed by using silver paste. The electrical resistivity was evaluated by using a reverse current method. For the I-V characteristic measurements, a pulse current is also applied by using a current source/monitor (ADCMT R6240B), in order to avoid self-heating of the single crystal. The thermoelectric power was measured by a differential method using a pair of thermocouples (chromel/Au + 7 at% Fe). The DC magnetizations were measured using a the SQUID magnetometer (MPMS3, Quantum Design, Inc.). The magnetization of the same single crystal (268 $\pm 2\mu$g) by applying a magnetic field of 10 kG in direction along the c-axis and perpendicular to the c-axis were measured.

Figure 2(a) shows the temperature dependence of electrical resistivity $\rho(T)$ and thermoelectric power $S(T)$ of a single crystal of $Ca_5Ir_3O_{12}$ along the c-axis. As is shown in Fig.2(a), $\ln\rho(T)$ exhibits a $(1/T)^{1/2}$ dependence above 130 K, which is known as variable range hopping for 1D systems or Efros-Shkloavskii variable range hopping; on the other hand, we obtained an energy gap of 0.177 eV by assuming Arrhenius law in the temperature range of 250-300 K. As this behavior is reported in previous researches, the present result is consistent with the previous results. The sharp bending in $\rho(T)$ at 105 K is also consistent with the previous results. At 300 K, the thermoelectric power $S(T)$ shows negative value of -55μV/K. On cooling, the absolute value of $S(T)$

decreases, and the sign changes to positive below 135 K. $S(T)$ shows a kink at 105 K. Above 105 K, $S(T)$ shows a dependence on $(1/T)^{1/4}$ rather than on $(1/T)^{1/2}$. From our preliminary Hall effect measurements on the polycrystalline sample, a negative Hall coefficient $R_H = -20\mathrm{cm}^3/\mathrm{C}$ was obtained at room temperature; the carrier density at room temperature is estimated to be $\sim 3\times10^{17}$ cm^{-3} for the single carrier model. These results indicate that the dominant carrier of $Ca_5Ir_3O_{12}$ is electron at room temperature. Figure 2(b) shows the temperature dependence of magnetization M/H along the c-axis and in the c-plane below 30 K. The M/H, both along the c-axis and in the c-plane indicate anomaly at 7.8 K; the difference between ZFC and FC is observed below 7.8 K. The magnetic anisotropy is consistent with that of the previous result.[15,16] Therefore, since the electrical and magnetic properties of our present single crystal are consistent with those of the previous results, we may consider that the present single crystals are good quality.

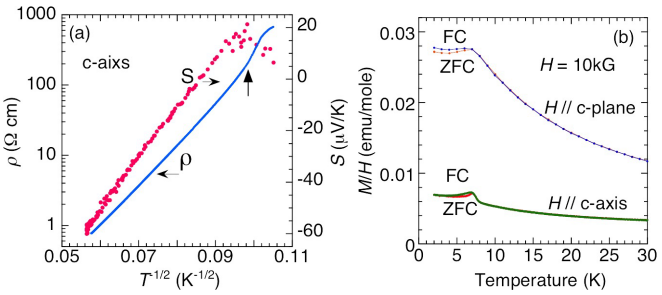

Fig. 2. (Color online) (a) Temperature dependence of electrical resistivity and thermoelectric power of a single crystal of $Ca_5Ir_3O_{12}$ along the c-axis. In this electrical resistivity measurement, the absolute value of applied current is fixed to 1 μA. (b) Magnetic susceptibility M/H of $Ca_5Ir_3O_{12}$ along the c-axis and in the c-plane, for temperatures below 30 K.

Next, we will demonstrate the nonlinear conductivity in the I-V characteristics of $Ca_5Ir_3O_{12}$. In the experiments on nonlinear conductivity, a relatively larger current is often applied in comparison with the standard resistivity measurements. It should be noted that the self-heating of a sample due to a large applied current may cause nonlinear conductivity. Therefore, the measurements of I-V characteristics of $Ca_5Ir_3O_{12}$ were performed by changing the amount of electric power applied to the sample by a pulse sweep method. The time dependence of current in the pulse sweep method is shown in the inset of Fig. 3(a). In the pulse sweep method, a pulse current with a width of T_w is applied during one period time of pulse sweep. After a delay time of T_d, from

the rise of current pulse to the voltage measurement, the voltage is measured during the measurement time $T_{\rm m}$. The voltage is measured again when the pulse current is zero. Then, their difference voltage is obtained. In a typical measurement, the period time of pulse sweep is 1 s, $T_{\rm W}$ is 310 ms, $T_{\rm d}$ is 1 ms, $T_{\rm m}$ is 0.5 ms, and the pulse interval is 10 s.

Figure 3(a) shows the I-V characteristics of $Ca_5Ir_3O_{12}$ at 110 K along the c-axis measured by the pulse sweep method with $T_{\rm d}$= 1, 2, 3, 5, 10, 20, 50, and 100 ms, and $T_{\rm m}$ = 0.5 ms with a pulse interval of 10 s. The I-V curve exhibits a strong $T_{\rm d}$ dependence. As $T_{\rm d}$ is increased, a reduction in voltage is observed above 0.4 mA. This indicates that the sample is heated by the pulse current during $T_{\rm d}$. Figure 3(b) shows the $T_{\rm d}$ dependence of voltage for a pulse current of 1.8 mA at 110 K and for a pulse current of 10 mA at 200 K. These data are fitted by the exponential decay $V(T_{\rm d}) = V_0 + V_1 \exp[-T_{\rm d}/\tau]$; the fitting curves with $(V_0, V_1, \tau) = (11.01\,{\rm V}, 3.696\,{\rm V}, 14.37\,{\rm ms})$ at 110 K and $(V_0, V_1, \tau) = (5.319\,{\rm V}, 0.9897\,{\rm V}, 22.21\,{\rm ms})$ at 200 K are shown. The results show that, when $T_{\rm d}$ is 1 ms and $T_{\rm m}$ is 0.5 ms, it is possible to obtain the data which the influence of self-heating of the sample is almost negligible; the error due to self-heating is 1% or less at the maximum current. The result for $T_{\rm d}$ = 1 ms in Fig. 3(a) clearly shows nonlinear conductivity. Therefore, we can conclude that this nonlinearity is not a trivial origin such as self-heating of the sample but an essential phenomenon.

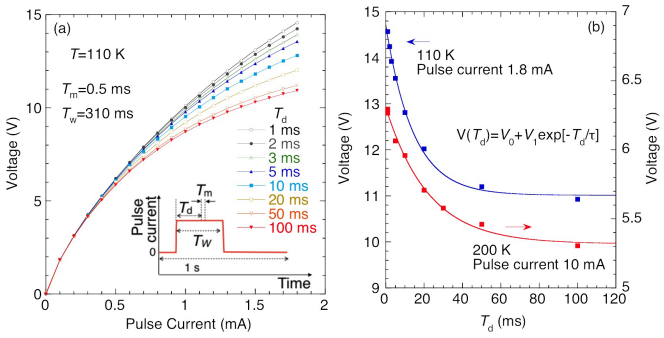

Fig. 3. (Color online) (a) I-V characteristic of single crystal $Ca_5Ir_3O_{12}$ at 110 K along the c-axis measured by the pulse sweep method with $T_{\rm d}$= 1, 2, 3, 5, 10, 20, 50, and 100 ms. Inset shows the time dependence of current in the pulse sweep. The pulse period is 1 s. The pulse sweeps are performed by setting the width of pulse current $T_{\rm W}$ = 310 ms, and $T_{\rm m}$ = 0.5 ms with a pulse interval of 10 s. (b) $T_{\rm d}$ dependence of voltage with a pulse current of 1.8 mA at 110 K and with a pulse current of 10 mA at 200 K for single crystal $Ca_5Ir_3O_{12}$ along the c-axis. The fitting curves by exponential decay are shown.

Figures 4(a) and 4(b) show the current density-electric field (J-E) curves of $Ca_5Ir_3O_{12}$ along the c-axis at 95, 110, 120, 150, 200, and 300 K, which were mea-

sured by the pulse sweep method with $T_{\rm d}$= 1 ms, $T_{\rm m}$ = 0.5 ms, and $T_{\rm W}$ = 310 ms, with a pulse interval of 10 s; we confirmed that this nonlinearity is reversible with the direction of current. It should be noted that the non-linear conductivity is observed at all the temperatures above the transition temperature of 105 K, for which measurements were taken. We could not confirm a negative resistance under the present measurement condition in which the voltage limit is 15 V. The J dependence of the resistivity ρ is shown in Fig. 4(c). ρ is derived by E/J from the data of Fig. 4(b). The inset shows the log-log plot of Fig. 4(c). On changing the current from 0.1 mA to 10 mA, ρ at 300 K is reduced by 44%. At low temperatures, the non-linearity of the resistivity becomes strong even at weak current densities. From the results of Fig. 4(c) and the inset, it can be seen that the J-E curve does not follow a power law and exponential function.

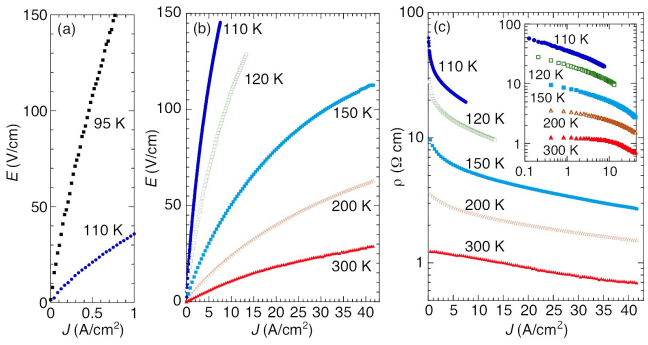

Fig. 4. (Color online) Current density - electric field ($J-E$) curve of $Ca_5Ir_3O_{12}$ along the c-axis (a) at 95 and 110 K, (b) at 110, 120, 150, 200, and 300 K, which were measured by a pulse sweep method with $T_{\rm d}$= 1 ms, $T_{\rm m}$ = 0.5 ms, and $T_{\rm W}$= 310ms with a pulse interval of 10 s. (b) Current density J dependence of resistivity ρ for $Ca_5Ir_3O_{12}$ along the c-axis at 110, 120, 150, 200, and 300 K. Inset shows the log-log plot of Fig.4(b).

To study the electronic structure of $Ca_5Ir_3O_{12}$, *ab initio* density functional calculations with plane-wave basis sets were performed using the `xTAPP` code,[18] where the ultrasoft pseudopotential[19,20] and the generalized gradient approximation (GGA) of the exchange-correlation potential[21] were employed. The cutoff energies in the wavefunction and charge densities were 64 and 256 Ry, respectively, and the SOI was explicitly considered. To study the effects of SOI, we performed the usual GGA calculation and compared it with the result including the SOI. Below, we refer to the former as GGA and to the latter as SO-GGA. The atomic and lattice parameters were optimized with an $8 \times 8 \times 8$ k-point sampling, and we found that SO-GGA reproduces the experimen-

tal crystal structure quite well. The Fermi-surface calculations were performed with the dense 21 × 21 × 63 k-point sampling to obtain the detailed surface structure.

Figure 5(a) shows our calculated band structure. To see the SOI effect, the SO-GGA band (thick red curves) is compared with the GGA band (thin blue curves) in Fig. 5(b). An appreciable difference can be observed in the low-energy bands; the GGA result exhibits metallic bands, particularly along the L-M or H-K lines. When the SOI is switched on, the metallic bands are split and a pocket-like band structure appears. The gap size for the SOI is about 0.3 eV, which is comparable to the valence bandwidth ∼0.5 eV.

Figures 5(c) and 5(d) show the Fermi surfaces based on the SO-GGA and GGA, respectively. We see that the GGA Fermi surface is contributed from the two bands (the dark-blue and bright-red colors), while the SO-GGA Fermi surface is basically formed by the one band; the SOI makes the right-red colored GGA Fermi surface disappear. In the SO-GGA Fermi surface, since the SOI resolves the band degeneracy, the Fermi surfaces are seemingly two but these two are originated from the same band. We thus depict the first and second Fermi surfaces with the dark-blue and bright-blue colors, respectively. Anyway, the observed vanishing of the GGA right-red colored Fermi surface indicates the reduction of the conduction channels, and thus the SOI would bring about the reduction of the metallic trend, which is consistent with the experimental data. However, it is not appropriate to discuss the observed semiconducting behavior in detail only by this calculation result. The anisotropy of resistivity reported in ref. 15 should be discussed by more elaborate calculation considering electron correlation and related quantum fluctuations explicitly.

In the SO-GGA Fermi surface, we see a sheet structure along the c^*-axis (the Γ-A line), indicating a nesting trend along this direction. We note that the SOI is relevant to narrowing the sheet separation of the blue-colored Fermi surfaces. The phonon calculation would be desirable in studying the Peierls instability of the low-energy state. In addition, the low-carrier state observed in the electron pockets of the SO-GGA band is easily affected by the several elementary excitations; for example, the plasma frequency can be small in the low-carrier density and such a low-energy plasmon excitation largely renormalizes the electronic structure.[22,23] The quantum fluctuation due to the local electronic interaction would also be relevant, which will be reinforced by the geometric frustration as is shown below.

We will discuss the nonlinear conductivity of $Ca_5Ir_3O_{12}$. In many materials, nonlin-

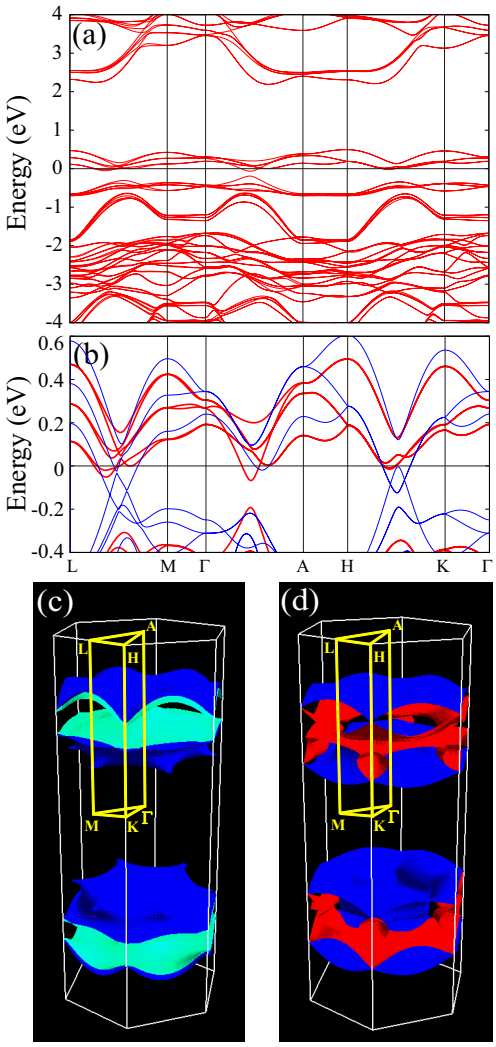

Fig. 5. (Color online) (a) *Ab initio* density functional band structure considering the SOI in $Ca_5Ir_3O_{12}$. The energy zero is the Fermi level. (b) Zoom of the low-energy band structure, where the SO-GGA result (thick red curves) is compared with the usual GGA result (thin blue curve). (c) Calculated Fermi surface for SO-GGA and (d) GGA. The SOI can resolve the band degeneracy, so we use the dark-blue and bright-blue colors to represent bands with the same band character. On the other hand, the GGA Fermi surface consists of two different bands (the dark-blue and dark-red colors). We note that the upper and lower objects in the panels (c) and (d) express the front and back sides at the surface, respectively. The Fermi surfaces were calculated with `FermiSurfer`.[24)]

ear conductivity is observed. In the case of low dimensional materials, the origin comes from the ordered state such as CDW, SDW, and charge-ordered phase.[25–27)] On the other hand, in some Ir and Ru oxides such as $BaIrO_3$ and Ca_2RuO_4, nonlinear conductivity is observed below their magnetic ordering temperature; a negative resistance is also observed.[28,29)] Although a nonlinear conductivity of Sr_2IrO_4 is also reported below

and above their antiferromagnetic ordering temperature, it is not clear whether the influence of self heating is fully considered in the experiments.[30] It should be noted that the nonlinear conductivity of $Ca_5Ir_3O_{12}$ is observed even in the non ordered state as clearly shown in Figs. 4(a) and 4(b). From the present result on electronic band structure, the nesting character along c^*-axis may be related to the nonlinear conductivity, which is comes from 1D chains of the edge-sharing IrO_6. In addition, $Ca_5Ir_3O_{12}$ has complex puzzles on the mixed valence state of Ir^{4+} and Ir^{5+}. As Ir^{4+} and Ir^{5+} exist in a ratio of 1:2 from the averaged valence of Ir ion, this situation can lead to the geometric frustration of electric charge on triangular lattice in both c-plane and 1D chains along c-axis. In order to reveal the transport properties of $Ca_5Ir_3O_{12}$, these puzzles need to be theoretically solved. Further experimental study on the conductivity in c-plane or under a higher electric field is also needed.

In summary, we have showed transport properties along c-axis in single crystal of $Ca_5Ir_3O_{12}$ with narrow band gap. We have discovered the nonlinear conductivity in the $I-V$ relationship in the non-ordered state. The resistivity decreases as the applied current becomes larger. The nonlinearity becomes stronger as temperature decreases. We have also showed *ab initio* density functional band structures and the Fermi surface. The estimated SOI is $\sim$0.3 eV, which is larger enough to be comparable to the valence bandwidth $\sim$0.5 eV. The SOI splits metallic bands and leads to a pocket-like band structure, thus reducing a metallic trend. The Fermi surface has a sheet structure along the c^*-axis, coming from the 1D chains structure of edge-sharing IrO_6.

The authors thank to Y. Motome for valuable discussions. This research was supported by ISSP Joint-Research program, and Promotion Project Uniting Strategic Program in Kyushu Institute of Technology. XRD measurements were performed at the Center for Instrumental Analysis in the Kyushu Institute of Technology. This research was partly supported by a Grant-in-Aid for Scientific Research (No.15H03692) from MEXT, Japan. KN acknowledges supports by Grants-in-Aid for Scientific Research (No.16K05452, 16H06345, 17H03379, 17H03393) from MEXT, Japan

References

1) B. J. Kim, Hosub Jin, S. J. Moon, J.-Y. Kim, B.-G. Park, C. S. Leem, Jaejun Yu, T. W. Noh, C. Kim, S.-J. Oh, J.-H. Park, V. Durairaj, G. Cao, and E. Rotenberg, Phys. Rev. Lett. **101**, 076402 (2008).

2) W. Witczak-Krempa, G. Chen, Y. B. Kim, and L. Balents, Annu. Rev. Condens. Matter Phys., **5**, 57, (2014).

3) B. J. Kim, H. Ohsumi, T. Komesu, S. Sakai, T. Morita, H. Takagi, T. Arima, Science, **323**, 1329 (2009).

4) A. Kitaev, Ann. Phys. **321** 2 (2006).

5) G. Jackeli and G. Khaliullin, Phys. Rev. Lett. **102**, 017205 (2009).

6) J. Chaloupka, G. Jackeli and G. Khaliullin, Phys. Rev. Lett. **105**, 027204 (2010).

7) Y. Machida, S. Nakatsuji, Y. Maeno, T. Tayama, T. Sakakibara, S. Onoda: Phys. Rev. Lett. **99**, 037203, (2007).

8) K. Matsuhira, M. Wakeshima, R. Nakanishi, T. Yamada, A. Nakamura, W. Kawano, S. Takagi and Y. Hinatsu: J. Phys. Soc. Jpn. **76** (2007) 043706.

9) K. Matsuhira, M. Wakeshima, Y. Hinatsu, and S. Takagi: J. Phys. Soc. Jpn. **80**, 094701 (2011).

10) F. Wang and T. Senthil, Phys. Rev. Lett. **106**, 136402 (2011).

11) Y.J. Yan, M. Q. Ren, H.C. Xu, B.P. Xie, R. Tao, H.Y. Choi, N. Lee, Y.J. Choi, T. Zhang, D.L. Feng, Phys. Rev. X **5**, 041018 (2015).

12) M. Wakeshima, N. Taira, Y. Hinatsu, Y. Ishii, Solid State Commun., **125**, 311 (2003).

13) R.F. Sarkozy, W. Moeller, B.L. Chamberland, J. Solid State Chem. **9**, 242 (1974).

14) K. Momma, and F. Izumi, J. Appl. Crystallogr. **44**, 1272 (2011).

15) G. Cao, V. Durairaj, S. Chikara, S. Parkin, and P. Schlottmann, Phys Rev. B, **75**, 134402 (2007).

16) The observed anisotropy is 1.2 times lager than the previous result in ref. 15.

17) I. Franke, P.J. Baker, S.J. Blundell, T. Lancaster, W. Hayes, F.L. Pratt, G. Cao, Phys Rev. B, **83**, 094416 (2011).

18) J. Yamauchi, M. Tsukada, S. Watanabe, and O. Sugino, Phys. Rev. B **54**, 5586 (1996).

19) D. Vanderbilt, Phys. Rev. B **41**, 7892 (1990).

20) K. Laasonen, A. Pasquarello, R. Car, C. Lee, and D. Vanderbilt, Phys. Rev. B **47**, 10142 (1993).

21) J. P. Perdew, K. Burke, and M. Ernzerhof, Phys. Rev. Lett. **77**, 3865 (1996).

22) K. Nakamura, S. Sakai, R. Arita, and K. Kuroki, Phys. Rev. B **88**, 125128 (2013).

23) K. Nakamura, Y. Nohara, Y. Yosimoto, and Y. Nomura, Phys. Rev. B **93**, 085124 (2016).

24) M. Kawamura, Y. Gohda, and S. Tsuneyuki, Phys. Rev. B **89**, 094515 (2014).

25) G. Grüner: *Density Waves in Solids* (Addison-Wesley, Reading, MA, 1994).

26) T. Yamaguchi, T. Konoike, K. Enomoto, M. Nishimura, T. Terashima, S. Uji, and H. M. Yamamoto, Phys. Rev. Lett. **96**, 136602 (2006).

27) S. Cao, J. Li, Z. Wang, H. Tian, Y. Qin, L. Zeng, C. Ma, H. Yang, and J. Li, Scientific Reports **2**, 330 (2012).

28) R. Okazaki, Y. Nishina, Y. Yasui, F. Nakamura, T. Suzuki and I. Terasaki, J. Phys. Soc. Jpn. **82**, 103702 (2013).

29) T. Nakano and I. Terasaki, Phys Rev. B **73**, 195106, (2006).

30) G. Cao, J. Bolivar, S. McCall, J.E. Crow, R.P. Guertin, Phys Rev. B **57**, R11039 (1998).